Mechanistic insights into bacterial metabolic reprogramming from omics-integrated genome-scale models

Noushin Hadadi[1*], Vikash Pandey[2], Anush Chiappino-Pepe[2], Marian Morales[1], Hector Gallart-Ayala[3], Florence Mehl[3], Julijana Ivanisevic[3], Vladimir Sentchilo[1] and Jan R. van der Meer[1]

[*]Corresponding author

[1]Department of Fundamental Microbiology, University of Lausanne, 1015 Lausanne, Switzerland

[2]Laboratory of Computational Systems Biotechnology, Ecole Polytechnique Fédérale de Lausanne (EPFL), 1015 Lausanne, Switzerland

[3]Metabolomics Platform, University of Lausanne, 1015 Lausanne, Switzerland

ABSTRACT

Understanding the adaptive responses of individual bacterial strains is crucial for microbiome engineering approaches that introduce new functionalities into complex microbiomes, such as xenobiotic compound metabolism for soil bioremediation. Adaptation requires metabolic reprogramming of the cell, which can be captured by multi-omics, but this data remains formidably challenging to interpret and predict. Here we present a new approach that combines genome-scale metabolic modeling with transcriptomics and exometabolomics, both of which are common tools for studying dynamic population behavior. As a realistic demonstration, we developed a genome-scale model of *Pseudomonas veronii* 1YdBTEX2, a candidate bioaugmentation agent for accelerated metabolism of mono-aromatic compounds in soil microbiomes, while simultaneously collecting experimental data of *P. veronii* metabolism during growth phase transitions. Predictions of the *P. veronii* growth rates and specific metabolic processes from the integrated model closely matched experimental observations. We conclude that integrative and network-based analysis can help build predictive models that accurately capture bacterial adaptation responses. Further development and testing of such models may considerably improve the successful establishment of bacterial inoculants in more complex systems.

INTRODUCTION

Microbiome engineering is an upcoming discipline that aims to manipulate, complement or restore the functionality of existing damaged communities, e.g., contaminated soils, by adding specific new metabolic capabilities[1]. A rational engineering approach requires a detailed understanding of general principles of the functioning of the microbial community and its physiological adaptations to perturbations, but such understanding is currently lacking and fragmentary[1,2]. The technically most simple way to provide new metabolic capacities to an existing microbial community is by strain addition (what one could call an *N+1* scenario)[3,4]. After an initial screening of the existing capacity of the microbial community, one or more preselected and well-characterized strains with the intended complementation could be prepared, formulated and inoculated into the community. Depending on the aims, such inoculants should maintain and reproduce for longer-term inside the resident community or only deploy their metabolic capacity transiently[3,4].

Inoculation of preselected strains has been widely practised for pollutant bioaugmentation, using bacteria with particular metabolic capabilities that enable them to efficiently degrade and grow on common pollutants such as toxic aromatic compounds[5]. However, even the simplest inoculations and N+1-strategies are rarely effective because it is insufficiently understood what inoculants need to establish successfully within a (new) existing community, and how they need to adjust their physiology to meet the requirements of the new environment and degrade the desired toxic compound(s). Modeling strategies based on the integration of a variety of (nowadays more easily) accessible condition-specific omics data, would help to better understand and predict how cellular regulation and physiology at different growth conditions and environments interplay. However, the impact and advantage of such integrative analysis are not yet explored to its full extent[6]. We propose and demonstrate here that combining comprehensive genome-wide transcriptomics, exometabolomics and metabolic modeling can better predict physiological adaptation.

Metabolic modeling has largely advanced through the development of GEnome-scale Metabolic models (GEMs) and constraint-based modeling techniques such as Flux Balance Analysis (FBA). GEMs can be built from the annotated genomes and they describe an organism's metabolism as

80 completely as possible, linking genotype to metabolic phenotypes[7]. GEMs encompass
81 metabolites, metabolic reactions, and genes coding for the enzymes catalyzing the reactions.
82 Together with FBA, GEMs predict steady-state fluxes[8,9], and therefore, they can predict cellular
83 physiology. While the genome specifies the complete set of biochemical reactions which the cell
84 can potentially carry out, the actual enzymatic capacity at each physiological condition is
85 orchestrated by regulatory networks in the cell. GEMs do not explicitly consider regulation,
86 whose effects are better reflected in the global transcriptome and the metabolome[10–14]. FBA
87 approaches have been extended with RNAseq and metabolomics data to capture cell regulation
88 and more accurately describe cellular metabolic behavior[15]. For example, transcriptional
89 regulation of gene expression has been linked to GEMs, either by taking into account the absolute
90 expression values, scoring genes and subsequently reaction fluxes as active or non-active based
91 on their expression,[16–18] or by incorporating relative gene-expression[14,18]. Use of relative gene
92 expression is assuming that the relative changes between two conditions correlate with the
93 resulting differential flux profiles. Both approaches can lead to condition-specific GEMs that are
94 more effective for inferring the actual biochemical activity and the observed physiology of the
95 microorganism.
96 As a study system for predicting physiology from an integrated GEM-transcriptome-metabolome
97 approach, we here use *Pseudomonas veronii* 1YdBTEX2. Strain 1YdBTEX2 is capable of degrading
98 a variety of mono-aromatic hydrocarbons such as benzene, toluene, ethylbenzene, and *m*- and
99 *p*-xylene (BTEX)[21–23]. The ability of *P. veronii* 1YdBTEX2 to grow in contaminated environments
100 makes it a promising candidate for rational complementation of microbial communities in
101 contaminated soils[24]. Based on an available manually curated high-quality genome[23], we
102 reconstructed the first GEM for *P. veronii* (iPsvr). Genome-wide transcription changes and
103 exometabolome compounds were measured during growth of *P. veronii* on toluene, in
104 exponential and in stationary phase. Transcriptome and exometabolome data were integrated
105 into the iPsvr using the recently developed tool *REMI* (Relative Expression and Metabolomics
106 Integrations)[20]. Two obtained metabolic models representing exponential and stationary
107 physiologies were then used to evaluate growth rates and the production of biomass precursors,
108 and model predictions were compared to the experimentally observed values. Although the

109 temporal variations of the growth rate cannot be predicted using GEMs[25], we showed that
110 introducing the additional regulatory information from gene expression and metabolomics data
111 into GEMs allows for consistently estimating growth rates at different growth phases. Finally, we
112 incorporated into iPsvr previously published transcriptomics data of *P. veronii* transits from liquid
113 culture to sand[23] to understand its physiological adaptation in soil. Our work shows strong
114 consistency of model outputs with the experimental data, manifesting that integration of
115 condition-specific omics data into a curated GEM constitutes a major improvement for prediction
116 of metabolic reprogramming during adaptation.
117

118 **RESULTS**

119 **Developing an integrated genomic-transcriptomic-metabolomic workflow**

120 To develop a pipeline that integrates genomics with transcriptomic and metabolomic data we
121 advanced in three stages: 1.) Quantify the cellular states at each unique growth phase by
122 genome-wide transcriptomics, and exometabolomic data from spent media composition (Fig.
123 1A); 2.) Construct a GEM for *P. veronii* strain 1YdBTEX2 (iPsvr), gap-fill missing parts of the
124 metabolism (compounds and reactions), complement genome annotation using the
125 transcriptomics and exometabolomic data and estimate the steady-state growth rate using FBA
126 (Fig. 1B); and 3.) Link the interrelationships between growth phases and the differentially
127 expressed genes and metabolite abundances by statistical inference and by REMI. The pipeline
128 generated two growth-phase-specific models, iPsvr-EXPO and iPsvr-STAT (Fig. 1C), which were
129 used to predict quantitative and dynamic readouts of *P. veronii* metabolism in both conditions
130 and in liquid-to-sand transition.

131 **Genome-wide gene expression and metabolite formation over time**

132 Whole-genome gene expression profiles and metabolite formation in the spent medium were
133 analyzed in *P. veronii* cultures growing in liquid minimal medium with toluene as sole carbon and
134 energy source, sampled at 0 h (T0h), 4 h (T4h, EXPO) and 24 h (T24h, STAT) after inoculation.
135 Genome-wide gene expression was quantified by mapping Illumina 100 nucleotide long single–
136 end sequencing reads from deeply sequenced cDNA libraries to the protein coding genes in *P.*
137 *veronii* genome (read numbers indicated in Table S1). For each sampling time point, four

138 replicates clustered closely together, with slightly higher variability observed among the T24h
139 replicates (Fig. S1A). A pair-wise comparison of expression levels showed that 1458 (818 up-
140 regulated and 640 down-regulated) out of the total 6943 genes (21%) were significantly
141 differentially expressed between EXPO and STAT phase cells, with at least 2-log fold-change
142 induction (false discovery rate [FDR]<0.05) (Fig. 2A, B).
143 *A priori*, based on the genome annotation, a subset of 1241 "metabolic genes" were used in the
144 GEM reconstruction (iPsvr). Out of these 1241, 300 (21%) were significantly differentially
145 expressed in EXPO vs. STAT phase cells (FDR<0.05) (Table S2). The transition to STAT phase in
146 bacteria is characterized by growth arrest in response to several factors, such as nutrient
147 depletion, the accumulation of toxic compounds and environmental stress, which decrease
148 ribosomal activity and therefore protein synthesis. As anticipated, enriched GO terms for the
149 category "Biological Process" among the differentially expressed genes between EXPO and STAT
150 included "protein folding" (GO:0006457), "tRNA aminoacylation for protein translation"
151 (GO:0006418), "intracellular protein transmembrane transport" (GO:0065002) and "regulation
152 of transcription, DNA-templated" (GO:0006355) (Table S3), thus indicating cells to be more active
153 in EXPO phase, as expected. Consistent with nutrients becoming depleted in STAT phase, the
154 terms "benzoate catabolic process via hydroxylation" (GO:0043640) and "tricarboxylic acid cycle"
155 (GO:0006099) (Table S3), important for aromatic compound catabolism, were under-
156 represented in the STAT phase transcriptome.
157 The untargeted metabolomic analyses of the spent medium detected 1630 (positively charged)
158 and 3509 (negatively charged) distinct ion species or metabolite features. Unsupervised principal
159 component analysis yielded three distinct clusters indicating metabolic phenotype
160 differentiation over time, from inoculum to stationary phase (Fig. S1B). Similar to the
161 transcriptomics data, a greater variability was observed among the T24h replicates.
162 Temporal patterns of annotated metabolites by HMDB database (accurate mass) matching[26]
163 showed a significant increase in the spent media over time of the majority of the metabolites
164 implicated in the toluene and benzene degradation pathways and central carbon pathways,
165 including glycolysis, purine and pyrimidine metabolism and amino acid metabolism (Fig. 2C). This
166 implies their production by the bacteria and progressive release into the media. One specific

167 group of metabolites, including citrate (C00158), glutamate (C00025), glutamine (C00064), and
168 aspartate (C00049), accumulated significantly in EXPO phase (T4h) in comparison to T0h,
169 followed by lower levels in STAT phase (Fig. 2C). This suggests their excretion in EXPO phase and
170 subsequent reconsumption when other nutrients became limiting (Fig. 2C).
171

172 **Genome-scale metabolic model (GEM) of *P. veronii* strain 1YdBTEX2 (iPsvr)**

173 A draft GEM was generated from the curated *P. veronii* genome[23] by using the RAVEN toolbox[27]
174 (Fig. 1B). The draft GEM was gap-filled by iterative manual curation until we obtained a model
175 able to carry non-zero flux through the biomass reaction at steady state. This signified cell
176 'growth', and indicated that the model was performing as expected for a biological system. The
177 cell biomass composition and compartment information were derived from two available models
178 of other Pseudomonads species: *P. putida*[28–30] and *P. stutzeri*[31] (see Methods). The reconstructed
179 iPsvr accounted for 1243 genes, 1812 metabolic reactions and 1677 metabolites localized within
180 two intracellular compartments, the cytosol and periplasm, and the extracellular environment
181 (Table 1).

182 The scope of iPsvr GEM was further widened by restoring the connectivity of the remaining
183 'blocked' reactions, i.e., isolated reactions that carry zero flux at any condition. To this end, we
184 explicitly considered the empirical gene-expression and exometabolomics data. We first used a
185 graph-based algorithm (see Methods) to decompose the iPsvr metabolic network into its main
186 subnetworks of 1370 reactions and 23 blocked reactions/pathways of different lengths, with the
187 longest blocked pathway consisting of seven reaction steps (Table S4). Out of 191 blocked
188 reactions/pathways, we identified those associated with differentially expressed genes between
189 the two growth conditions and the ones whose participating metabolites were present in the
190 exometabolomic data. The identified reactions/pathways were next unblocked by gap-filling as
191 described in the Methods section. Interestingly, we identified gap-filling reactions that had been
192 annotated to *P. veronii* genes with RAVEN but had a lower score than the ones chosen as a
193 baseline for the draft reconstruction of iPsvr. The gap-filling algorithm introduced 50 new
194 metabolic reactions together with their corresponding 26 genes to iPsvr (Table 1 and Table S5).
195

196 **Table 1**: iPsvr components in the final GEM.

Genes	
from annotation	1243
added for gap-filing	26
Reactions	
metabolic reactions	1812
- from annotation	1762
- added for gap-filing	50
transport reactions	243
exchange reactions	219
Metabolites	
intracellular compounds	1677
extracellular compounds	219
cellular building blocks	65

197

198 The experimentally determined maximum specific growth rate of *P. veronii* strain 1YdBTEX2 in
199 minimal medium with toluene as the sole carbon source was in the range of 0.25 h^{-1} to 0.35 h^{-1}.
200 Computational prediction of the growth rate on toluene from the curated iPsvr using
201 thermodynamics-based flux balance analysis (TFA)[8,32,33], which integrates thermodynamic
202 constraints into FBA, yielded 0.91 h^{-1} (at a maximum allowed toluene uptake rate of of 5.5 mmol
203 gDW^{-1} h^{-1}, and without considering transcriptomics and metabolomics information, see Methods
204 section).

205

206 **Omics-based curation and gap-filling in iPsvr for toluene degradation and phenylalanine**
207 **metabolism**

208 Given the importance of toluene degradation by *P. veronii* 1YdBTEX2, we manually curated the
209 predicted toluene (Fig. 3A) and phenylalanine metabolic pathways (Fig. 3B) to ensure they were
210 fully functional in iPsvr. Toluene is converted in *P. veronii* via (1S,2R)-3-methylcyclohexa-3,5-
211 diene-1,2-diol to 3-methylcatechol, which is further degraded, according to the KEGG pathway
212 database[34], through two pathways until the central carbon metabolism compounds are reached
213 (Fig. 3A and Fig. S2). The iPsvr growth simulation on minimal media containing toluene as the
214 sole carbon source showed that the pathway producing pyruvate and acetaldehyde in four
215 reaction steps was functional (1.13.11.2, 3.7.1.-, 4.2.1.8 and 4.1.3.39 in Fig. S2), which has

216 experimentally been shown to be the main toluene degradation route in *P. veronii*[23]. In contrast,
217 the second functional pathway (Fig. 3A)[23], was blocked in iPsvr because it lacked the enzyme
218 2.8.3.6 (highlighted in red in Fig. 3A), and it was therefore disconnected from the main metabolic
219 subnetwork. We found that three out of the six genes in this pathway (PVR_r1g5041,
220 PVR_r1g5042, PVR_r1g1440) were more than 2-fold differentially expressed between the two
221 growth conditions (highlighted in green in Fig. 3A), which further suggested that this pathway is
222 indeed active in *P. veronii*. Homology-based BLAST searches[35] of the gene sequences of 2.8.3.6
223 against the *P. veronii* genome identified the corresponding gene for catalyzing this reaction
224 (PVE_r1g3867, e-value of 10^{-20}, to *scoA*). Note that the default e-value in RAVEN is 10^{-50}, which is
225 why the reaction was not initially captured in the model from the genome annotation. Therefore,
226 the missing reaction (2.8.3.6) was added to iPsvr, and the toluene pathway (Fig. 3A) was
227 connected to the rest of the metabolic network through the Krebs cycle and carried flux.
228 The phenylalanine metabolic pathway was gap-filled using the exometabolomic data (Fig. 3B).
229 Three out of the eight reaction steps of this pathway (4.1.1.28, 1.14.14.54 and 1.14.13.-) were
230 initially missing in iPsvr, leading to a dead-end pathway without flux. Four metabolites of
231 phenylalanine metabolism were detected in the exometabolomics data (colored in blue in Fig.
232 2B), one of which, 2-hydroxyphenylacetate, was absent in the iPsvr GEM. This suggested that
233 phenylalanine metabolism should proceed via 2-hydroxyphenylacetate in *P. veronii* (Fig. 3B). The
234 enzyme producing 2-hydroxyphenylacetate from phenylacetaldehyde (1.14.14.54) was found by
235 BLAST (PVE_r1g94, e-value of 10^{-20} to CYP504), added to iPsvr and could thus link both
236 metabolites. The next step (1.14.13.-), yielding homogentisate (Fig. 3B) was also added, but no
237 protein sequence could be assigned, as it corresponds to an orphan reaction (KEGG reaction ID:
238 R05450). The first enzyme (4.1.1.28), which decarboxylates L-phenylalanine to phenethylamine,
239 must be present, given the detection of both compounds in the exometabolomics data, although
240 no *P. veronii* protein sequence could be identified through BLAST search.
241
242 **Omics integration into iPsvr**
243 REMI (Relative Expression and Metabolomics Integrations) was used to integrate the relative
244 gene-expression and metabolite abundance data between EXPO and STAT into iPsvr. We

245 explored three scenarios, depending on the type of data integrated into iPsvr: (i) REMI-TGex for
246 the integration of relative gene-expression data only; (ii) REMI-TM for the integration of
247 metabolomics data only; and (iii) REMI-TGexM for the simultaneous integration of both the gene-
248 expression and metabolite abundance data into a thermodynamically curated model. The "T" in
249 the three methods stands for the inclusion of thermodynamic constraints. Contextualized
250 metabolic models (iPsvr-EXPO and iPsvr-STAT) coherent with omics data were built, and the
251 growth rates were again simulated (Table 2).
252 342 out of a total of 352 (97%) integratable gene-expression and metabolite abundance data
253 points could be consistently included in REMI; the remaining 3% being inconsistent (Table 2, third
254 row). Simulated growth rates for EXPO phase under the condition of integrating both gene-
255 expression and metabolomics data (REMI-TGexM) were the closest to the experimentally
256 observed rates (0.40 h^{-1} for REMI-TGexM versus 0.25–0.35 h^{-1}, Table 2).
257 The integration of exometabolomics data alone (REMI-TM) was insufficient, with a predicted
258 growth rate of 0.86 h^{-1} , which is close to the rate of 0.91 h^{-1} that was obtained for the
259 unconstrained iPsvr model (Table 2). The integration of relative gene-expression data alone
260 (TGex) yielded an *in silico* exponential growth rate of 0.48 h^{-1} , which is close to the REMI-TGexM
261 value (Table 2). Both REMI-TGex and REMI-TGexM, but not REMI-TM, correctly estimated near
262 zero growth rates (0.06 h^{-1} and 0.07 h^{-1}, respectively) for stationary phase cells (Table 2).
263

264 **Table 2**: Summary of the REMI results of the relative integration of exometabolomics (REMI-
265 TM), gene expression (REMI-TGeX) and both datasets (REMI-TGeXM) into iPsvr. Theoretical
266 maximum consistency score, TMCS; Maximum consistency score, MCS; Std, standard deviation.

Method	Score		Growth rate (h^{-1})	
	TMCS	MCS	EXPO	STAT
TFA	-	-	0.91*	0.91*
REMI-TM	215	123	0.86	0.67
REMI-TGeX	618	229	0.48	0.06
REMI-TGexM	833	342	0.40	0.07
Experimental	-	-	0.31 (std=0.05)	0

267 **by definition, there is no difference between the simulated growth rate at different growth*
268 *phases in FBA simulations.*
269

270 **Analysis of the biomass precursor production at different growth phases**

271 To understand the underlying mechanisms of growth reduction when cells transit from EXPO to
272 STAT, we identified the biomass precursors that may become limiting in the stationary phase,
273 therefore leading to growth arrest. The 65 biomass precursors were grouped into seven groups
274 of biomass building blocks (BBBs), namely carbohydrates, cofactors and vitamins, DNA
275 nucleotides, lipids, minerals, amino acids, and RNA nucleotides. For each metabolite, we
276 calculated the log2 fold-change of their maximal production between EXPO and STAT using REMI-
277 TGex and REMI-TGexM (Table S6).

278 Both REMI-TGex and REMI-TGexM indicated large variations in the production of BBBs between
279 the two phases (Fig. 4), the maximal relative change occurring in the production of cofactors and
280 vitamins. Out of the 20 precursors that were classified as cofactors and vitamins, the production
281 of 10 (REMI-TGexM) and 18 (REMI-TGex) of them was at least 2-log fold-change higher in iPsvr-
282 EXPO than in iPsvr-STAT (Table S6). Rather surprisingly, an increased production of certain BBBs
283 occurred in STAT. Both REMI-TGex and REMI-TgexM predicted that several amino acids, e.g.,
284 tyrosine and lysine, and some lipids, e.g., hexadecanoic acid, had at least a 2-log fold-change
285 higher production in STAT (Fig. 4A & B). As before, the variant with integration of only
286 exometabolomic data (REMI-TM) did not predict any significant differences in the production of
287 BBBs between EXPO and STAT culture (Table S6).

288

289 ***P. veronii* adaptation from liquid culture to the soil as growth environment**

290 Finally, as an additional validation of our approach, we predicted the *in silico* physiology for *P.*
291 *veronii* during adaptation to the soil environment, using a previously published genome-wide
292 transcriptome data set of cells exposed for 1 h to liquid medium or to sand, with either toluene
293 or succinate as carbon substrate[23].

294 Integrating the transcriptomic data[23] into iPsvr using REMI-TGex, produced *in silico* growth rates
295 of 0.52 and 0.66 h^{-1} for toluene or succinate in liquid medium. Remarkably, the model predicted
296 strong reduction of growth rate upon transition to the sand, i.e., from 0.52 h^{-1} to 0.23 h^{-1}
297 (toluene) and 0.66 h^{-1} to 0.07 h^{-1} (succinate). This suggests that cells have to adapt to soil as their
298 new environment and have to reprogram their physiology before resuming growth. The higher

299 reduction of growth in case of succinate is in agreement with experimental results in the previous
300 study[23] , and can be explained from the lower concentration of succinate than toluene available
301 in the soil, therefore rapidly used by the cells and leading to nutrient starvation.
302 To understand how the transition from liquid medium to sand constrains the metabolic fluxes
303 and impacts growth of *P. veronii*, we analyzed the production of BBBs in both growth
304 environments. Intrestingly, we observed the same robust reduction in the production of
305 cofactors and vitamins upon transition to sand in the case of succinate, as had been predicted
306 for transition to STAT in liquid culture (14 out of 20 precursors with more than 2-log fold lower
307 production). In contrast, in case of cells exposed to toluene in sand only 8 of the cofactor and
308 vitamin precursors were 2-log fold lower expressed. The higher number of precursors with lower
309 production rates might thus explain the stronger growth arrest in case of succinate during
310 transition to sand as opposed to toluene. In contrast, the production of other precursor BBBs,
311 such as phosphatidylcholine and ubiquinone-8, similarly increased in sand both for toluene and
312 succinate (Fig. S3 A&B). "This suggests that the cells in sand reshape their membrane content
313 and respiratory pathways
314
315 **DISCUSSION**
316 This work demonstrates how a metabolic-model-based (multi)omics data integration approach
317 can accurately capture cell physiology and adaptation during growth or environmental
318 transitions. Metabolic models are typically used for predicting optimal cell growth, but not for
319 growth transitions and adaptation. We show here the usefulness of models with
320 comprehensively integrated transcriptomics and exometabolomic to capture changes in growth
321 rate during adaptation. As example, we studied transition of the toluene-degrading bacterium *P.*
322 *veronii* 1YdBTEX2 from exponential growth to stationary phase, and during adaptation from
323 liquid to a sand environment.
324 For the purpose of this study, we reconstructed and curated the first genome-scale metabolic
325 model of *P. veronii*, iPsvr. iPsvr is useful for a wide range of applications in biological and
326 biotechnological research, such as the integration of omics data, investigation of relationships
327 among species in microbial communities, bioremediation strategies, design of metabolic

328 engineering strategies, hypothesis-driven discovery, and analysis of metabolic network
329 properties. As such, iPsvr may represent a valuable resource for the study of complex
330 microbiomes and microbiome engineering.
331
332 GEMs usually contain inconsistencies that manifest as blocked reactions, i.e., the reactions that
333 carry zero flux. Most of the available metabolic models are gap-filled to obtain a functional model
334 that produces all the BBBs. Nevertheless, many reactions in GEMs are not directly connected to
335 biomass formation and may remain blocked even after routine gap-filling. Roughly, 20–50% of
336 the reactions of published GEMs are blocked reactions[36,37]. For example, in the most recently and
337 best-curated published *E. coli* model, iML1515, 10% of the reactions are blocked[38]. We identified
338 the blocked reactions/pathways in iPsvr and introduced a novel omics-based gap-filling
339 approach, which targets the gap-filling of reactions/pathways by looking at differentially
340 expressed genes or metabolites. We showed that the gap-filling step improved the metabolic
341 model connectivity, thus increasing the number of functional pathways that can carry flux. The
342 curation also increased the consistency of the metabolic model with the omics data, expressed
343 as the number of genes/metabolites with available omics data that can be integrated into iPsvr.
344 We illustrated through two gap-filling examples on toluene and phenylalanine metabolism how
345 we could add the missing parts of metabolism and increase consistency.
346 Statistical analysis of gene expressions and metabolite levels revealed significant variations
347 across the exponential and stationary phase, exemplifying the known distinct physiologies under
348 these conditions. However, the system's level physiology and the underlying adaptation
349 mechanisms remained unrevealed.
350
351 It should be highlighted that in FBA, the growth rate is evaluated under the assumption that all
352 metabolic fluxes in the cell are geared towards the maximal production of biomass at each
353 moment of the cell growth and under any environmental condition. Nevertheless, inclusion of
354 REMI[20], a method for the integration of omics data into metabolic models and for building
355 context-specific models, produced more accurate predictions of *P. veronii* growth rates under
356 dynamic conditions. Integration of the transcriptomic data (as in REMI-TGex and –TGexM) proved

357 to be vital for improving growth rate predictions, whereas inclusion of metabolomic data alone
358 (as in REMI-TM) was insufficient. This might be expected, because only a small subset of
359 metabolites could be putatively identified, such that their impact on the predictions was
360 comparatively smaller. The estimated growth rate was slightly closer to the experimentally
361 measured values in the case of REMI-TGexM, which combines transcriptomics and metabolomics
362 data. Overall, these results clearly demonstrated that integrating multi-omics data in GEMs
363 significantly increases the consistency of the model predictions with experimental observations.
364
365 REMI-iPsvr analysis suggested *P. veronii* adapts to STAT phases primarily by limiting the
366 metabolic fluxes for the production of the majority of cofactors and vitamins required for growth,
367 with metabolism reshuffling being regulated at the transcriptional level. In addition, an increased
368 production of specific amino acids in STAT phase suggests the cell is preparing for starvation and
369 survival. Similar to the EXPO to STAT transition, the production of most of the BBBs decreased in
370 cells inoculated in sand compared to liquid culture, which explains the overall observed reduction
371 in growth rates. In contrast, the production of several precursors from the *cofactors and vitamins*,
372 and the BBBs *amino acids* actually increased in cells transited to sand, both for sand with toluene
373 or succinate. We hypothesize that these BBBs are needed to adapt to the local sand conditions.
374 This finding is in agreement with work of Morales et al.[23], who concluded from Gene Ontology
375 terminology that *P. veronii* cells inoculated in sand readjusted their metabolism during the first
376 hour of contact.
377 Collectively, our results demonstrate the importance of integrating into metabolic models the
378 contextualization of condition-specific gene-expression and metabolite-abundance data. This
379 increases the value of growth rate predictions and improves the assessment of the relative
380 changes of measurable metabolic phenotypes. The method as demonstrated here is thus an
381 important advancement to explain, quantify or predict cellular responses to environmental or
382 genetic perturbations, which is crucial for microbiome engineering.
383
384
385

386 **METHODS**

387 **Culture conditions for *P. veronii* transcriptome and exometabolomic studies**

388 *P. veronii* 1YdBTEX2 was grown on solid 21C mineral medium[39] with toluene in the vapor phase
389 at 30°C for 3 days. Colonies were inoculated into three 100 ml screw-cap conical flasks containing
390 25 ml of the mineral medium amended with 0.5 ml of a 1:19 mixture of toluene:tetradecane
391 (Sigma-Aldrich ref: 34866; Aldrich ref: 87140). Flasks were incubated at 30°C and at 180 rpm on
392 an orbital shaker until a culture turbidity (OD_{600}) of 0.7 (mid-exponential growth phase). At this
393 point, the three cultures were pooled, and the bacterial cells were harvested by centrifugation
394 (swing-out rotor A-4-44, Eppendorf; 3220 g, 8 min, 30°C). The cell pellet was resuspended in the
395 mineral medium and centrifuged again, as described above, to remove any residual carbon. After
396 that, the cells were resuspended in mineral medium, diluted to obtain a starting OD_{600} of 0.16
397 and transferred into four replicate flasks, to which the toluene:tetradecane mix was added, as
398 described above. The cultures were incubated at 30°C and 180 rpm and regularly sampled for OD
399 measurements. For transcriptomics, approximately 1×10^9 cells were harvested from an
400 appropriate volume of the culture by centrifugation at 3,500 g, for 6 min at 30°C; snap-frozen in
401 liquid nitrogen and stored at -80°C until RNA extraction. Three quadruplicate sample sets were
402 produced: the inoculum at time 0 (T0h), that is cells starved for approximately 30 min at 25°C in
403 mineral medium without a carbon source; exponentially growing cells (at $OD_{600} \approx 0.5$, harvested
404 after 4 h of incubation in the toluene-amended mineral medium); stationary phase cells (at
405 $OD_{600} \approx 1.8–1.9$ harvested after 24 h incubation). To study the composition of the
406 exometabolome (metabolites in the culture medium excreted or leaked out of cells), 1 ml of the
407 culture was sampled at the same time points. Cell culture was transferred into a 1.5 ml
408 polypropylene microcentrifuge tube, which was clarified by 20 min centrifugation at 21,100 *g*
409 and 4°C, after which 0.5 ml of spent media was transferred to a new polypropylene tube, stored
410 at -80°C and shipped on dry ice to the metabolomics facility.

411

412 **RNA extraction, RNA-seq library preparation and sequencing**

413 Total RNA from the frozen cell pellets was extracted using the RNA PowerSoil Total RNA Isolation
414 Kit (MoBio Laboratories) as recommended by the manufacturer. Contaminating genomic DNA

415 was removed by two cycles of TURBO DNase (Invitrogen) digestion and RNeasy MinElute Cleanup
416 kit (QIAGEN) column purification. The quantity, purity and integrity of RNA samples were
417 assessed using agarose gel electrophoresis, NanoDrop spectrophotometer (ThermoFisher
418 Scientific) measurements and Agilent 2100 Bioanalyser (Agilent Technologies) profiling.
419 The completeness of DNA removal was verified by PCR using primers Pv_chr2_fw,
420 ATCGGCTGTCCGACATCGGACG and Pv_chr2_rev, TCGAAGAGCTCCACCGAGAGCCGCC) and 1 pg of
421 genomic DNA as a positive control, as described previously[23]. Next, 4 µg of each RNA sample were
422 depleted from ribosomal RNAs, converted to the reverse-complement stranded Illumina
423 sequencing library using the ScriptSeq Complete Kit (Bacteria, Illumina) and indexed with
424 ScriptSeq™ Index PCR primers set 1 (Epicentre, Illumina) following the standard protocol. The
425 resulting directional RNA-seq libraries were sequenced using single-end 100-nt read chemistry
426 on an Illumina HiSeq 2500 platform (Illumina) at the Lausanne Genomic Technologies Facility.
427
428 **Untargeted LC-HRMS metabolomics**
429 The spend media (100 µL) samples collected at different time points were extracted with 400 µL
430 of ice-cold methanol to quench the metabolism, precipitate proteins and extract a broad range
431 of polar metabolites. The extracted media were analyzed by HILIC-HRMS using an electrospray
432 ionization source operating in both positive and negative mode. Pooled QC samples
433 (representative of the entire sample set) were analyzed periodically (every 4 samples)
434 throughout the entire analytical run in order to assess the quality of the data, correct the signal
435 intensity drift and remove the peaks with poor reproducibility (CV > 30%) that can be considered
436 chemical or bioinformatic noise. Data were acquired using a 1290 UHPLC system (Agilent
437 Technologies) interfaced with a 6550 iFunnel Q-TOF mass spectrometer operating in a full-scan
438 MS mode. In addition, pooled QC samples were analyzed in auto MS/MS mode (i.e. Data
439 Dependent Analysis [DDA]) to acquire the MS/MS data for metabolite identification. In positive
440 mode, chromatographic separation was carried out using an Acquity BEH Amide, 1.7 µm, 100 mm
441 × 2.1 mm I.D. column (Waters, Massachusetts, US). The mobile phase was composed of A = 20
442 mM ammonium formate and 0.1% formic acid in water and B = 0.1% formic acid in acetonitrile.
443 A linear gradient elution from 95% B (0–1.5 min) down to 45% B (17–19 min) was applied

444 followed by 5 min for column re-equilibration to the initial gradient conditions. The flow rate was
445 400 µL/min, column temperature 30°C and sample injection volume 2 µl. ESI source conditions
446 were set as follows: dry gas temperature 290°C and flow 14 L/min, fragmentor voltage 380 V,
447 sheath gas temperature 350°C and flow 12 L/min, nozzle voltage 0 V, and capillary voltage 2000
448 V. In negative mode, a SeQuant ZIC-pHILIC (100 mm, 2.1 mm I.D. and 5 µm particle size; Merck,
449 Damstadt, Germany) column was used. The mobile phase was composed of A = 20 mM
450 ammonium acetate and 20 mM NH_4OH in water at pH 9.3 and B = 100% acetonitrile. The linear
451 gradient elution ran from 90% (0–1.5 min) to 50% B (8–11 min) down to 45% B (12–15 min).
452 Finally, the initial chromatographic conditions were established during a 9 min post-run for
453 column re-equilibration. The flow rate was 300 µL/min, column temperature 30°C and sample
454 injection volume 2 µl. ESI source conditions were set as follows: dry gas temperature 290°C and
455 flow 14 L/min, sheath gas temperature 350°C, nebulizer 45 psi and flow 12 L/min, nozzle voltage
456 0 V, and capillary voltage 2000 V.
457 In the MS-only mode, the instrument was set to acquire over the m/z range 50–1200, with the
458 MS acquisition rate of two spectra/s. Targeted MS/MS data for dysregulated metabolite features
459 were acquired using the inclusion list with narrow isolation window (≈ 1.3 *m/z*), MS acquisition
460 rate of 500 ms, and MS/MS acquisition rate of 500 ms.
461
462 **Data processing and statistical analysis**
463 *Transcriptomics*: Read mapping, sorting and formatting of the raw reads was done with Bowtie2[40]
464 and Samtools[41], using the finalized gapless *P. veronii* 1YdBTEX2 genome sequence as in Morales
465 et al[23]. Mapped reads were counted with HTSeq[42], then further processed and analyzed with
466 edgeR[43]. Only reads counted more than once per million in at least three replicates were kept.
467 After normalization of the counts, transcript abundances were compared in pairwise conditions
468 in a modified Fischer exact test (as implemented in edgeR). Genes were called significantly
469 differentially expressed between two EXPO and STAT when their false-discovery rate was <0.05
470 and their fold-change >2 and were subsequently interpreted using Gene Ontology (GO) analysis.
471 GO terms of *P. veronii* genes were inferred using the program BLAST2GO[44]. The same software

472 was then used to analyze GO data sets of significantly differentially expressed genes in each pair-
473 wise comparison, under the TopGO "Weight" algorithm.
474 *Metabolomics*: Raw LC-MS data were converted to mzXML files using ProteoWizard MS Convert.
475 mzXML files were uploaded to XCMS for data processing including peak detection, retention time
476 correction, profile alignment, and isotope annotation. Data were processed as a multi-group
477 experiment, and the parameter settings were as follows: centWave algorithm for feature
478 detection (Δm/z = 20 ppm, minimum peak width = 5 sec and maximum peak width = 30 sec, S/N
479 threshold = 6, mzdiff = 0.01, integration method = 1, prefilter peaks = 3 prefilter intensity = 1000,
480 noise filter = 0), obiwarp settings for retention time correction (profStep = 1), and parameters for
481 chromatogram alignment, including mzwid = 0.015, minfrac = 0.5 and bw = 5.5. Preprocessed
482 data (following the signal-intensity drift correction and noise removal with the "batchCorr" R
483 package) were filtered according to the p-value (< 0.05) and signal intensity (> 1000 ion counts).
484 The remaining table of metabolite features together with the most significant ion features
485 selected from the loadings plot of the multivariate models in positive and negative ionization
486 mode were subjected to metabolite identification as described below.
487 In the first instance, putative metabolite identification was performed by accurate mass and
488 retention time (AMRT) matching against an in-house database (containing information on 600
489 polar metabolites from the Mass Spectrometry Metabolite Library Supplied by IROA
490 Technologies, Sigma-Aldrich, characterized under the same analysis conditions). For that, raw
491 data files (.d) were processed using Profinder B.08.00 software (Agilent Technologies) with the
492 following parameter settings: mass tolerance 10 ppm, retention time tolerance 0.2 min, height
493 filter 1000 counts, and peak spectrum obtained as an average of scans at 10% of the peak. In
494 parallel, the XCMS output table of significantly different metabolite features was matched
495 against the Human Metabolome Database (HMDB)[26] based on accurate mass (AM) with Δppm =
496 10. The list of hits was further manually curated by taking into account the biological relevance
497 of the hit (endogenous vs. exogenous metabolites) and a presence of the "true" peak shape
498 (using the interactive XCMS Online interface[45]). Short listed ions of interest together with the
499 metabolites identified by the in-house database were further subjected to targeted MS/MS
500 validation. The metabolite identifications were validated by matching the MS/MS[46] data acquired

501 in the pooled samples (for each experiment in each LC-MS analysis mode) against the in-house
502 PCDL database, METLIN (https://metlin.scripps.edu/) standard metabolite database[47] or
503 mzCloud (https://www.mzcloud.org/). Otherwise, if the MS/MS data quality did not allow for
504 metabolite ID confirmation, the metabolite IDs remained putative, based only on accurate mass
505 matching.
506
507 **Genome-scale model reconstruction**
508 The *P. veronii* 1YdBTEX2 genome-scale metabolic reconstruction process combines the
509 automated draft metabolic network process with several manual refinements and curation
510 procedures, in total involving four main steps: **(i) functional annotation of the genome**:
511 functional annotation of the genome is required prior to the reconstruction of the GEMs, and
512 consequently, the quality of a GEM highly depends on the availability of a gapless genome. The
513 protein sequences (FASTA files) of *P. veronii* 1YdBTEX2 were acquired from a previously published
514 study[23] and were annotated to identify the associated reactions that enzymes catalyze to
515 determine the stoichiometric matrix, done using the RAVEN Toolbox[27]. The generation of the
516 draft metabolic network followed the protocol detailed previously[27,48,49], and the output of this
517 annotation process is summarized in Table S6. Version 1.07 of the RAVEN Toolbox and the version
518 of KEGG database as of September 2017 were used. **(ii) Compartmentalization, the definition of**
519 **biomass reaction and uptakes and secretions:** In the absence of information or experimental
520 evidence about the compartmentalisation and the cell content in *P. veronii* 1YdBTEX2, the cell
521 compartment information (i.e., cytosol and periplasm), the transport mechanism between the
522 compartments and the extracellular environment, the uptakes and secretions, and the biomass
523 composition were obtained from two available models of closely related Pseudomonads*:*
524 *Pseudomonas putida*[28–30] and *Pseudomonas stutzeri*[31]. The biomass reaction in a GEM designates
525 the metabolic precursors that build the BBBs, i.e., DNA, RNA, amino acids, lipids and
526 carbohydrates and their corresponding stoichiometric coefficients. **(iii) Thermodynamic**
527 **curation:** In a thermodynamically curated model, the standard Gibb's free energy of a reaction
528 and consequently the directionality of the reactions, i.e., reversible or irreversible, are associated
529 with the reaction as additional constraints, which allow the performance of TFA. We followed the

530 established protocol to thermodynamically curate metabolic models[32,33] to add thermodynamics
531 constraints to iPsvr, where we could estimate the standard Gibb's free energy of formation of
532 76% metabolites, using the group contribution method (GCM)[50] and the standard Gibb's free
533 energy of 84% of metabolic reactions in iPsvr. This allowed us to perform TFA, simulate the
534 growth and determine whether iPsvr was functional, with further evaluations if it correctly
535 predicted the expected growth-associate phenotypes. **(iv) Gap-filling of iPsvr:** The draft
536 metabolic network of iPsvr did not contain all the necessary reactions for the production of all
537 the biomass building blocks, and thus, the model did not show any growth. This is a very common
538 observation in the reconstruction process of GEMs, since the (automatic) genome annotations
539 are often incomplete or erroneous, with significant proportion of predicted proteins having no
540 functions attributed[51]. Therefore, reactions without associated genes were included in order to
541 obtain a functional model that simulates non-zero growth, done using a procedure called gap-
542 filling. We followed the gap-filling procedure introduced previously[48], wherein the production of
543 each biomass precursor is defined as a metabolic task[27] and a mixed-integer linear programming
544 (MILP) formulation is used to generate alternative groups of minimal number of reactions
545 (borrowed from KEGG) that enable the production of the biomass precursor. The draft GEM was
546 gap-filled by iterative manual curation until a model was obtained that was able to carry non-
547 zero flux through the biomass reactions at steady state (i.e., signifying 'growth'). Although gap-
548 filling is a routine procedure in the curation of GEMs and most of the available GEMs are gap-
549 filled to obtain a functional model that is able to grow under defined conditions, gaps in pathways
550 not involved with biomass production are, however, mostly overlooked in GEM analysis. We
551 performed a complementary second gap-filling step apart from the biomass reaction, where as
552 a result, the consistency of iPsvr with the obtained experimental data on gene expression and
553 metabolomics was increased. Available GEMs usually contain a large well-connected
554 subnetwork, which encompasses the most of the central carbon metabolism and a part of the
555 secondary metabolism, and many isolated reactions (or sets of reactions) are probably
556 disconnected from the rest of the network because of misannotations or insufficiently known
557 pathways. Such isolated reactions/pathways are blocked, i.e., cannot carry flux under any
558 condition, and therefore one or more reactions must be added to connect the blocked reactions

559 with the rest of the metabolic network. To this end, the metabolic network structure of iPsvr was
560 decomposed to the main component and to the isolated (disconnected) reactions/pathways
561 using a MATLAB graph-based built-in function (conncomp). Using the same gap-filling approach,
562 the blocked reactions/pathways that were associated with differentially expressed genes (in the
563 pair-wise comparison of exponential- and stationary-phase datasets) or measured metabolites in
564 exometabolomic data were gap-filled to become functional in the model (carry non-zero flux).
565
566 **Omics data integration**
567 REMI[20] was used for the integration of transcriptomics and exometabolomics data into iPsvr.
568 REMI assumes that reaction fluxes associated with genes that are significantly differentially
569 expressed are deregulated. Moreover, REMI also considers that the *in vivo* metabolite abundance
570 ratios between the two conditions, e.g., the two growth phases can be used to constrain reaction
571 fluxes associated with the metabolites that are differentially regulated. Expression/abundance-
572 based ratios between the two conditions are formulated as flux perturbations for each reaction
573 and are imposed as constraints on individual fluxes. Based on the data used, it translates into
574 three different methods: (i) REMI-TGex allows the integration of relative gene expression data
575 into a thermodynamically curated GEM, (ii) REMI-TM allows the integration of metabolomics
576 data and (iii) REMI-TGexM integrates simultaneously both the gene expression and metabolite
577 abundance data as additional constraints into the metabolic model.
578 REMI aims to maximize consistency between differential expression and fluxes as well as
579 differential metabolite concentrations and fluxes. To study condition-specific differences in
580 metabolism between two conditions (perturbed *vs* reference), REMI considers a separate
581 metabolic model for each condition. Then, to integrate differential expression, REMI enforces a
582 higher flux through a reaction in the perturbed condition (perturbed model) as compared to a
583 reference condition (reference model) if the genes of the reaction are upregulated. For
584 downregulated reactions, REMI enforces a lower flux as compared to a reference. To integrate
585 extracellular metabolite concentrations, REMI assumes that if a metabolite is upregulated, then
586 the production of the metabolite is forced to be higher as compared to a reference condition,
587 and similarly, a lower production of a metabolite is forced if a metabolite is found to be

588 downregulated. Then, an optimization problem is formulated to maximize the number of
589 constraints imposed by the relative gene expression and metabolite abundances that can be
590 integrated into the model while preserving a growth phenotype. Two scores are calculated: a
591 theoretical maximum consistency score (TMCS), representing the number of genes/metabolites
592 with available omics data, and the maximum consistency score (MCS), representing the number
593 of genes/metabolites whose relative omics data are consistent with relative network fluxes and
594 therefore can be integrated in the model.
595 The MILP formulation enables enumerating alternative sets (size equal to MCS) from a given set
596 of constraints. The most consistent models are built by activating constraints that are overlapping
597 and consistent between all the alternatives.
598 We used the transcriptomics and/or exometabolomics datasets measured at the exponential and
599 stationary phase and also at the sand versus liquid environment, to derive additional flux
600 constraints for the TFA problem, which were applied using REMI.
601
602 **Thermodynamics-based flux analysis (TFA) and the analysis of the biomass building blocks**
603 To determine fluxes and subsequently the growth rate at different growth and environmental
604 conditions using iPsvr, we employed FBA, the most widely used constraint-based modeling
605 technique for studying biochemical networks and cellular physiology. Previous studies show that
606 the integration of appropriate thermodynamic constraints leads to more accurate metabolic
607 model predictions and also a significant reduction in the ranges of the predicted fluxes (solution
608 space)[8,32]. We perform TFA for estimating the growth rate before and after the integration of
609 omics data.
610 We further identified the biomass building blocks (BBB), wherein a low/zero production limits
611 growth upon the transition of cells from the exponential to stationary phase or from liquid to the
612 soil environment (two examples that were discussed in this work). Each BBB was tested by
613 defining the TFA objective function as the maximum production of that metabolite under the
614 defined media condition (the same for all the BBBs). Then, the BBB production was compared
615 and the limiting BBBs for each case were identified.
616

ACKNOWLEDGMENTS

This work was supported by SystemsX.ch, and evaluated by the Swiss National Science Foundation, within grant 2013/158 (Design and Systems Biology of Functional Microbial Landscapes 'MicroScapesX'). The author would like to thank Dr. Ljubisa Miskovic for constructive criticism of the manuscript and for his careful proof-reading.

REFERENCES

1. Sheth, R. U., Cabral, V., Chen, S. P. & Wang, H. H. Manipulating Bacterial Communities by in situ Microbiome Engineering. *Trends Genet.* **32**, 189–200 (2016).
2. Stenuit, B. & Agathos, S. N. Deciphering microbial community robustness through synthetic ecology and molecular systems synecology. *Curr. Opin. Biotechnol.* **33**, 305–317 (2015).
3. Buffie, C. G. *et al.* Precision microbiome reconstitution restores bile acid mediated resistance to Clostridium difficile. *Nature* (2015). doi:10.1038/nature13828
4. De Roy, K., Marzorati, M., Van den Abbeele, P., Van de Wiele, T. & Boon, N. Synthetic microbial ecosystems: an exciting tool to understand and apply microbial communities. *Environmental microbiology* (2014). doi:10.1111/1462-2920.12343
5. Adams, G. O., Fufeyin, P. T., Okoro, S. E. & Ehinomen, I. Bioremediation, Biostimulation and Bioaugmention: A Review. *Int. J. Environ. Bioremediation Biodegrad.* **3**, 28–39 (2015).
6. Robaina-Estévez, S. & Nikoloski, Z. On the effects of alternative optima in context-specific metabolic model predictions. *PLOS Comput. Biol.* **13**, e1005568 (2017).
7. Lewis, N. E. *et al.* Omic data from evolved E. coli are consistent with computed optimal growth from genome-scale models. *Mol. Syst. Biol.* (2010). doi:10.1038/msb.2010.47
8. Henry, C. S., Broadbelt, L. J. & Hatzimanikatis, V. Thermodynamics-based metabolic flux analysis. *Biophys. J.* **92**, 1792–805 (2007).
9. Orth, J. D., Thiele, I. & Palsson, B. Ø. What is flux balance analysis? *Nat. Biotechnol.* **28**, 245–8 (2010).
10. Johnson, C. H., Ivanisevic, J. & Siuzdak, G. Metabolomics: beyond biomarkers and

646 towards mechanisms. *Nat. Rev. Mol. Cell Biol.* **17**, 451–459 (2016).
647 11. Richelle, A., Joshi, C. & Lewis, N. E. Assessing key decisions for transcriptomic data
648 integration in biochemical networks. doi:10.1101/301945
649 12. Töpfer, N., Kleessen, S. & Nikoloski, Z. Integration of metabolomics data into metabolic
650 networks. *Front. Plant Sci.* **6**, 49 (2015).
651 13. Pinu, F. R. & Villas-Boas, S. G. Extracellular Microbial Metabolomics: The State of the Art.
652 *Metabolites* **7**, (2017).
653 14. Pinu, F. R. *et al.* Metabolite secretion in microorganisms: the theory of metabolic
654 overflow put to the test. *Metabolomics* **14**, 43 (2018).
655 15. O'Brien, E. J., Lerman, J. A., Chang, R. L., Hyduke, D. R. & Palsson, B. Genome-scale
656 models of metabolism and gene expression extend and refine growth phenotype
657 prediction. *Mol. Syst. Biol.* (2013). doi:10.1038/msb.2013.52
658 16. Navid, A. & Almaas, E. Genome-level transcription data of Yersinia pestis analyzed with a
659 New metabolic constraint-based approach. *BMC Syst. Biol.* **6**, 150 (2012).
660 17. Töpfer, N., Jozefczuk, S. & Nikoloski, Z. Integration of time-resolved transcriptomics data
661 with flux-based methods reveals stress-induced metabolic adaptation in Escherichia coli.
662 *BMC Syst. Biol.* (2012). doi:10.1186/1752-0509-6-148
663 18. Collins, S. B., Reznik, E. & Segrè, D. Temporal Expression-based Analysis of Metabolism.
664 *PLoS Comput. Biol.* (2012). doi:10.1371/journal.pcbi.1002781
665 19. Navid, A. & Almaas, E. Genome-level transcription data of Yersinia pestis analyzed with a
666 New metabolic constraint-based approach. *BMC Syst. Biol.* **6**, 150 (2012).
667 20. Pandey, V., Hadadi, N. & Hatzimanikatis, V. Enhanced flux prediction by integrating
668 relative expression and relative metabolite abundance into thermodynamically
669 consistent metabolic models. *PLOS Comput. Biol.* (2019).
670 doi:10.1371/journal.pcbi.1007036
671 21. De Lima-Morales, D. *et al.* Draft Genome Sequence of Pseudomonas veronii Strain
672 1YdBTEX2. *Genome Announc.* (2013). doi:10.1128/genomeA.00258-13
673 22. De Lima-Morales, D. *et al.* Degradation of benzene by Pseudomonas veronii 1YdBTEX2
674 and 1YB2 is catalyzed by enzymes encoded in distinct catabolism gene clusters. *Appl.*

675 *Environ. Microbiol.* (2016). doi:10.1128/AEM.03026-15
676 23. Morales, M. *et al.* The genome of the toluene-degrading Pseudomonas veronii strain
677 1YdBTEX2 and its differential gene expression in contaminated sand. *PLoS One* **11**, 1–21
678 (2016).
679 24. Trigo, A., Valencia, A. & Cases, I. Systemic approaches to biodegradation. *FEMS*
680 *Microbiol. Rev.* **33**, 98–108 (2009).
681 25. Adadi, R., Volkmer, B., Milo, R., Heinemann, M. & Shlomi, T. Prediction of microbial
682 growth rate versus biomass yield by a metabolic network with kinetic parameters. *PLoS*
683 *Comput. Biol.* **8**, e1002575 (2012).
684 26. Wishart, D. S. *et al.* HMDB: The human metabolome database. *Nucleic Acids Res.* (2007).
685 doi:10.1093/nar/gkl923
686 27. Agren, R. *et al.* The RAVEN Toolbox and Its Use for Generating a Genome-scale Metabolic
687 Model for Penicillium chrysogenum. *PLoS Comput. Biol.* (2013).
688 doi:10.1371/journal.pcbi.1002980
689 28. Nogales, J., Palsson, B. & Thiele, I. A genome-scale metabolic reconstruction of
690 Pseudomonas putida KT2440: iJN746 as a cell factory. *BMC Syst. Biol.* (2008).
691 doi:10.1186/1752-0509-2-79
692 29. Puchałka, J. *et al.* Genome-scale reconstruction and analysis of the Pseudomonas putida
693 KT2440 metabolic network facilitates applications in biotechnology. *PLoS Comput. Biol.*
694 (2008). doi:10.1371/journal.pcbi.1000210
695 30. Yuan, Q. *et al.* Pathway-Consensus approach to metabolic network reconstruction for
696 pseudomonas putida KT2440 by systematic comparison of published models. *PLoS One*
697 (2017). doi:10.1371/journal.pone.0169437
698 31. Babaei, P., Marashi, S.-A. & Asad, S. Genome-scale reconstruction of the metabolic
699 network in Pseudomonas stutzeri A1501. *Mol. BioSyst.* **11**, 3022–3032 (2015).
700 32. Ataman, M., Hatzimanikatis, V., Betenbaugh, M. J. & Bentley, W. E. Heading in the right
701 direction: thermodynamics-based network analysis and pathway engineering. *Curr. Opin.*
702 *Biotechnol.* **36**, 176–182 (2015).
703 33. Salvy, P. *et al.* pyTFA and matTFA: A Python package and a Matlab toolbox for

704 Thermodynamics-based Flux Analysis. *Bioinformatics* (2018).
705 doi:10.1093/bioinformatics/bty499
706 34. Kanehisa, M., Furumichi, M., Tanabe, M., Sato, Y. & Morishima, K. KEGG: New
707 perspectives on genomes, pathways, diseases and drugs. *Nucleic Acids Res.* (2017).
708 doi:10.1093/nar/gkw1092
709 35. Altschul, S. F., Gish, W., Miller, W., Myers, E. W. & Lipman, D. J. Basic local alignment
710 search tool. *J. Mol. Biol.* (1990). doi:10.1016/S0022-2836(05)80360-2
711 36. Ravikrishnan, A. & Raman, K. Critical assessment of genome-scale metabolic networks:
712 The need for a unified standard. *Brief. Bioinform.* (2015). doi:10.1093/bib/bbv003
713 37. Ponce-De-Leon, M., Calle-Espinosa, J., Peretó, J. & Montero, F. Consistency Analysis of
714 Genome-Scale Models of Bacterial Metabolism: A Metamodel Approach. *PLoS One*
715 (2015). doi:10.1371/journal.pone.0143626
716 38. Monk, J. M. *et al.* iML1515, a knowledgebase that computes Escherichia coli traits.
717 *Nature Biotechnology* (2017). doi:10.1038/nbt.3956
718 39. Gerhardt, P., Wood, W.A., Krieg, N.R., Murray, R. *Methods for General and Molecular*
719 *Bacteriology*. *American Society for Microbiology* (1994).
720 40. Langmead and Steven L Salzberg. Bowtie2. *Nat. Methods* (2013).
721 doi:10.1038/nmeth.1923.Fast
722 41. Li, H. *et al.* The Sequence Alignment/Map format and SAMtools. *Bioinformatics* (2009).
723 doi:10.1093/bioinformatics/btp352
724 42. Anders, S., Pyl, P. T. & Huber, W. HTSeq-A Python framework to work with high-
725 throughput sequencing data. *Bioinformatics* (2015). doi:10.1093/bioinformatics/btu638
726 43. Robinson, M. D., McCarthy, D. J. & Smyth, G. K. edgeR: A Bioconductor package for
727 differential expression analysis of digital gene expression data. *Bioinformatics* (2009).
728 doi:10.1093/bioinformatics/btp616
729 44. Conesa, A. *et al.* Blast2GO: A universal tool for annotation, visualization and analysis in
730 functional genomics research. *Bioinformatics* (2005). doi:10.1093/bioinformatics/bti610
731 45. Gowda, H. *et al.* Interactive XCMS online: Simplifying advanced metabolomic data
732 processing and subsequent statistical analyses. *Anal. Chem.* (2014).

733 doi:10.1021/ac500734c
734 46. Mylonas, R. *et al.* X-rank: A robust algorithm for small molecule identification using
735 tandem mass spectrometry. *Anal. Chem.* (2009). doi:10.1021/ac900954d
736 47. Tautenhahn, R. *et al.* An accelerated workflow for untargeted metabolomics using the
737 METLIN database. *Nat. Biotechnol.* (2012). doi:10.1038/nbt.2348
738 48. Chiappino-Pepe, A., Tymoshenko, S., Ataman, M., Soldati-Favre, D. & Hatzimanikatis, V.
739 Bioenergetics-based modeling of Plasmodium falciparum metabolism reveals its essential
740 genes, nutritional requirements, and thermodynamic bottlenecks. *PLoS Comput. Biol.*
741 (2017). doi:10.1371/journal.pcbi.1005397
742 49. Thiele, I. & Palsson, B. Ø. A protocol for generating a high-quality genome-scale
743 metabolic reconstruction. *Nat. Protoc.* **5**, 93–121 (2010).
744 50. Jankowski, M. D., Henry, C. S., Broadbelt, L. J. & Hatzimanikatis, V. Group contribution
745 method for thermodynamic analysis of complex metabolic networks. *Biophys. J.* (2008).
746 doi:10.1529/biophysj.107.124784
747 51. Schnoes, A. M., Brown, S. D., Dodevski, I. & Babbitt, P. C. Annotation error in public
748 databases: Misannotation of molecular function in enzyme superfamilies. *PLoS Comput.*
749 *Biol.* (2009). doi:10.1371/journal.pcbi.1000605
750
751
752
753
754
755
756
757
758
759

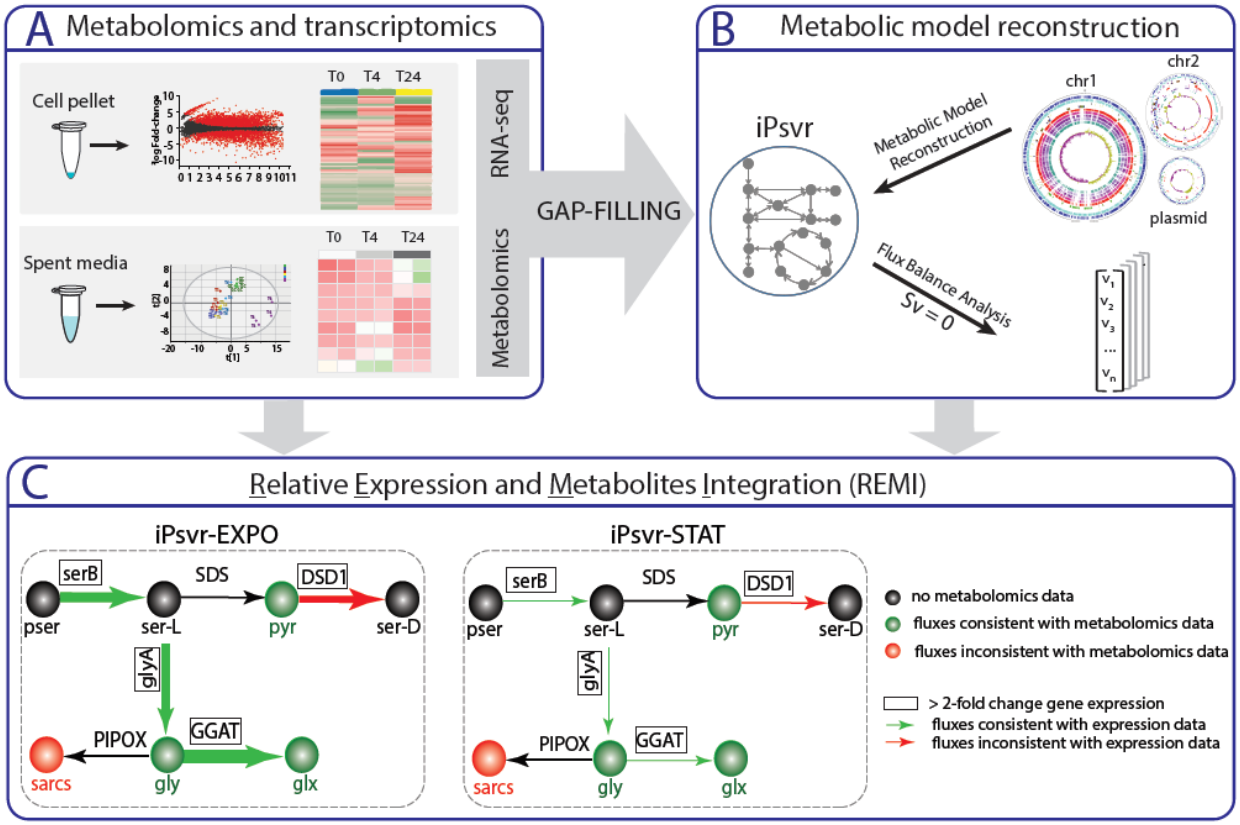

Figure 1: Schematic overview of the integrated genomic-transcriptomic-metabolomic pipeline applied in this study. (A) Stage 1: Relative gene expression and exometabolomic data were determined and analyzed, and these data were used to gap-fill iPsvr at blocked reactions. (B) Stage 2: A genome-scale metabolic model (GEM) of *P. veronii* strain 1YdBTEX2, iPsvr, was reconstructed and flux-balance analysis (FBA) was performed to simulate the growth of the cell. (C) Stage 3: Additional relative differential gene expression and metabolite abundance data were integrated into the metabolic model with REMI and physiology-specific models were built. Here, the REMI methodology is illustrated on a section of inferred iPsvr glycine, serine and threonine metabolism and iPsvr-EXPO (exponential phase) and iPsvr-STAT (stationary phase) as the two physiology-specific models. Significantly differentially expressed genes (here, *serB*, *glyA*, DSD1 and GGAT) are outlined in boxes. The thickness of arrows designates the fold-change in estimated fluxes, where green arrows indicate consistency with the gene-expression fold-change values, and the red ones inconsistencies. Measured metabolite concentrations (here: pyr, sarcs, gly and glx) are indicated in green if the values are consistent with estimated fluxes and in red otherwise. Phosphoserine phosphatase, SerB; Serine hydroxymethyltransferase, GlyA; D-serine dehydratase, DSD1; Glyoxylate aminotransferase, GGAT; Pyruvate, pyr; Sarcosine, sarcs; Glycine, gly; Glyoxylate, glx.

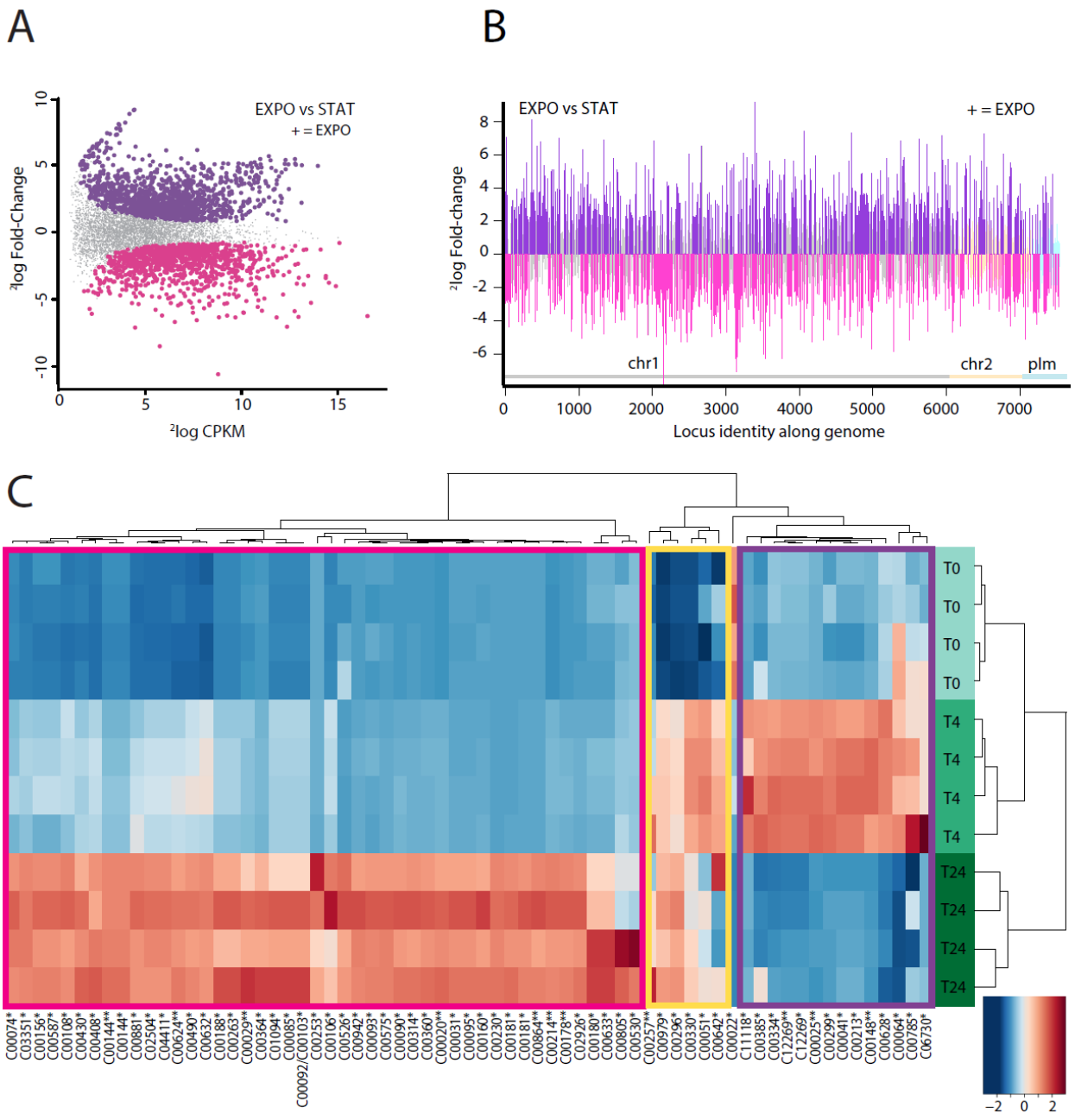

Figure 2: **Genome-wide gene-expression and metabolite abundance differences in *P. veronii* 1YdBTEX in exponential (EXPO) relative to stationary (STAT) phase.** (A) Smear-plot of global gene expression intensity (2log counts per kilobase per million, CPKM) versus expression changes (2log fold change) in EXPO vs. STAT. In grey, genes not statistically differentially expressed (logFC<1, FDR>0.05, P>0.01); magenta, genes with lower, and dark purple, genes with higher expression in EXPO (+). (B) Differential expression per gene between EXPO and STAT plotted as a function of genomic location (chromosome 1, chr1; chromosome 2, chr2; and plasmid, plm; organized according to locus_tag number). Bars indicate 2log-fold change, dark purple and pink denote statistically significant higher and lower expressed genes in EXPO, respectively. (C) Heatmap of 164 metabolites annotated with their KEGG IDs showing clustering at different

culture sampling time points. Metabolites are clustered (x-axis) in three major groups (left to right): (i) accumulation at T24h (STAT) (pink box), (ii) accumulation at T4 continued to T24 (yellow box), and (iii) accumulation at T4h (EXPO) followed at depletion at T24h (STAT) (purple box).

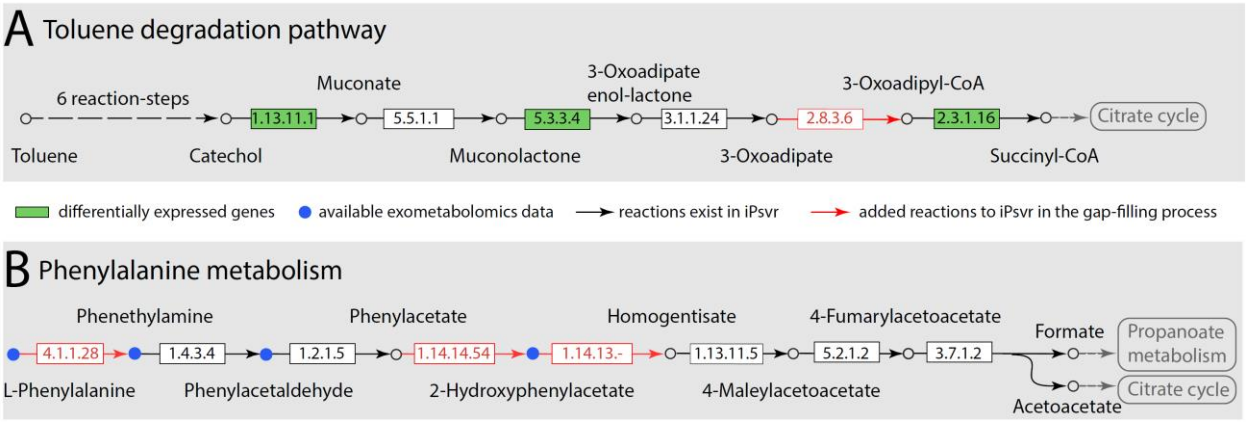

Figure 3: Gap filling of two blocked pathways in iPsvr based on the gene expression and exometabolomics data. (A) One of the two toluene degradation pathways in *P. veronii* (from the KEGG pathway database[34]) involved one missing enzyme (highlighted in red), and three genes (highlighted in green) differentially expressed between the exponential and stationary growth conditions. (B) The phenylalanine metabolic pathway involved three missing enzymes (highlighted in red) and four metabolites (highlighted in blue) identified in the exometabolomic data.

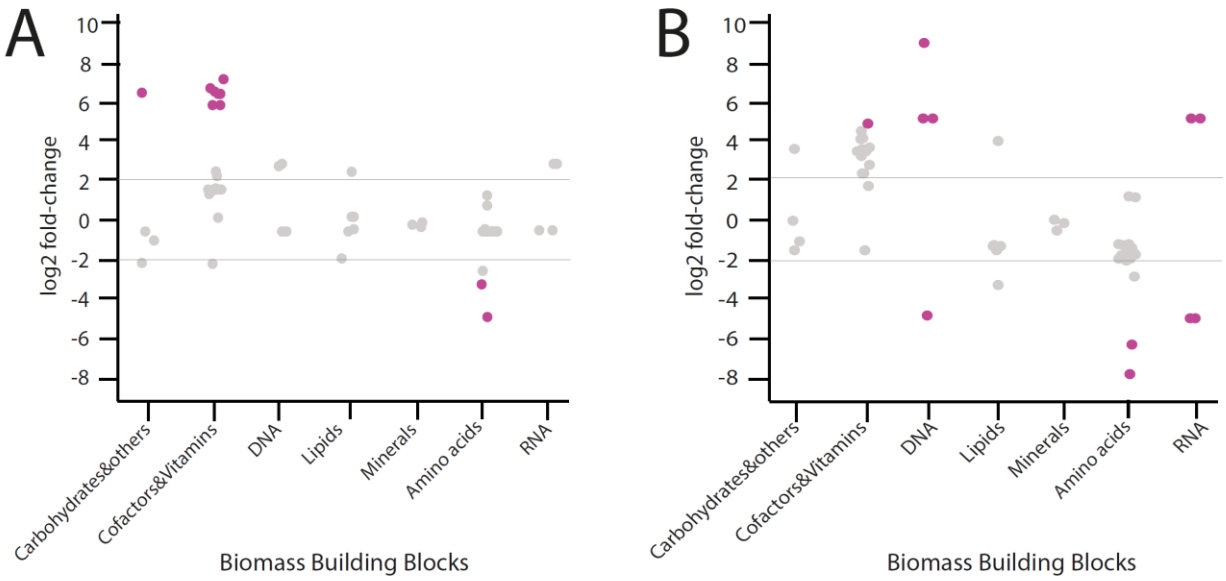

Figure 4: **Differential *in silico* production (mmol/gDW/h) of seven biomass building block groups between the exponential and stationary growth phase.** (A) Integration of relative gene expression data (EXPO vs STAT) using REMI-TGexM. (B) Integration of relative gene expression and exometabolomics data (EXPO vs STAT) using REMI_TGex. Each dot in the graph represents the individual biomass precursors within that category and the statistically significant changes (p=value < 0.05) are highlighted in purple. For BBB group statistics, see Table S7.

SUPPLEMENTARY FIGURES

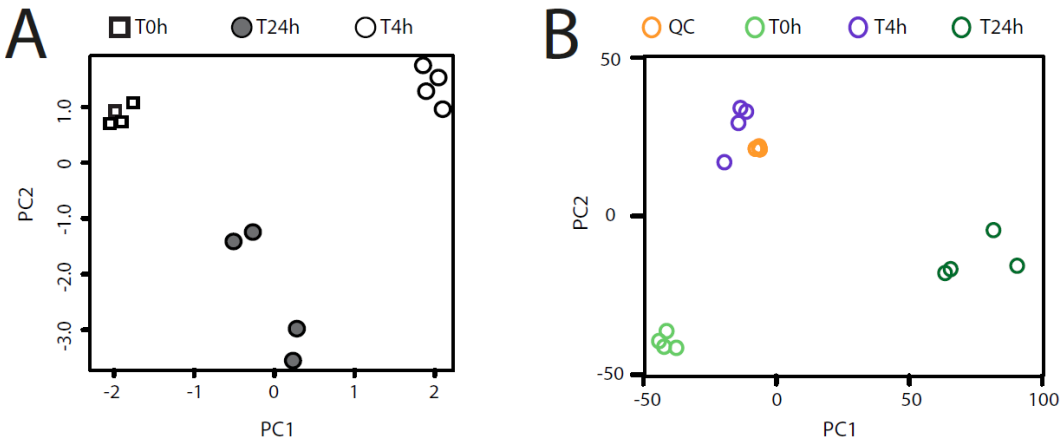

821 **Supplementary Figure 1: Principal component analysis of** (A) quadruplicate global RNA-
822 sequencing data sets of *P. veronii* 1YdBTEX2 after 4 h, 24 h and the 0 h control (T0) and (B) of
823 exometabolomics data, grouped QC samples of T0, T4 and T24 samples.

824

825

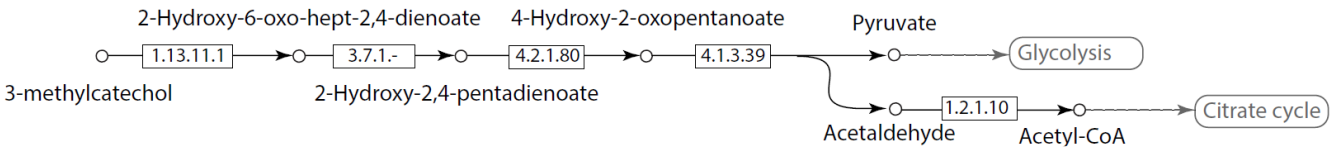

826

827 **Supplementary Figure 2: Main functional toluene degradation pathway branch in iPsvr.** 3-
828 methylcatechol is converted to pyruvate and acetaldehyde, which are further involved in
829 central carbon pathways.

830

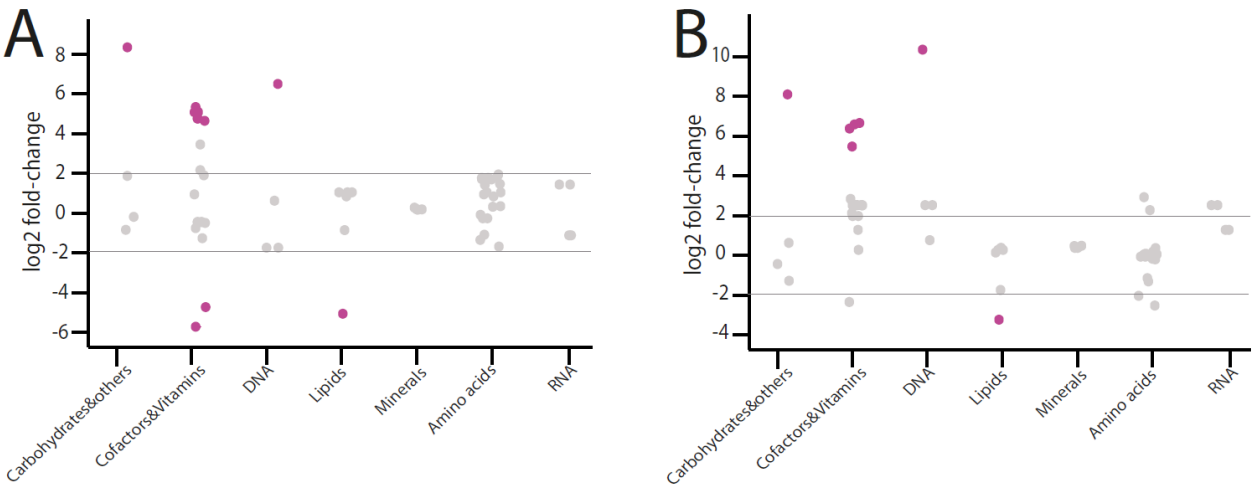

831

832 **Supplementary Figure 3: Differential *in silico* production (mmol/gDW/h) of seven biomass**
833 **building block groups between cells in liquid medium and sand.** (A) Integration of relative gene
834 expression data (liquid vs sand) using REMI-TGex when cells grow on Toluene . (B) Integration of
835 relative gene expression data (liquid vs sand) using REMI-TGex when cells grow on Succinate.
836 Each dot in the graph represents the individual biomass precursors within that category and the
837 statistically significant changes (p=value < 0.05) are highlighted in purple. For BBB group statistics,
838 see Table S7.

839

840

841 **SUPPLEMENTARY TABLES** (given as an excel file and each excel sheet is a Supplementary Table)

842 **Table S1.** Summary of RNA-seq yields of the different time points.

843 **Table S2.** Significantly differentially expressed metabolic genes in EXPO vs. STAT

844 **Table S3.** Under-represented Biological processes in STAT vs EXPO.

845 **Table S4.** iPsvr network decomposition into its main subnetwork and isolated
846 reactions/pathways.

847 **Table S5.** Gap-filled reactions introduced into the iPsvr with their corresponding genes.

848 **Table S6.** Differential *in silico* production (mmol/gDW/h) of biomass precursors, grouped in
849 seven biomass building block groups, between the exponential and stationary growth phase
850 using REMI-TGexM, REMI-TGex and REMI-TM.

851 **Table S7.** Statistical test for BBB groups. Significant up- or down-regulations (p=value < 0.05)
852 are highlighted in red.

Main component reactions

R00005
R00006
R00009
R00013
R00014
R00019
R00021
R00022
R00025
R00026
R00036
R00066
R00078
R00081
R00084
R00086
R00093
R00094
R00103
R00114
R00115
R00130
R00131
R00137
R00150
R00158
R00160
R00161
R00174
R00177
R00182
R00183
R00189
R00190
R00192
R00196
R00197
R00199
R00200
R00203
R00207
R00214
R00217
R00220
R00221

R00226
R00227
R00228
R00230
R00235
R00236
R00237
R00238
R00239
R00243
R00245
R00248
R00253
R00256
R00258
R00259
R00260
R00264
R00267
R00268
R00274
R00282
R00286
R00287
R00289
R00294
R00299
R00310
R00315
R00316
R00318
R00332
R00341
R00344
R00345
R00351
R00353
R00355
R00357
R00360
R00361
R00369
R00371
R00372
R00374
R00396
R00401

R00405
R00409
R00410
R00411
R00416
R00425
R00426
R00428
R00430
R00448
R00451
R00462
R00465
R00470
R00472
R00475
R00479
R00480
R00481
R00485
R00486
R00490
R00494
R00497
R00508
R00509
R00511
R00512
R00515
R00524
R00525
R00527
R00529
R00548
R00549
R00552
R00566
R00568
R00570
R00571
R00573
R00575
R00578
R00582
R00586
R00597
R00602

R00604
R00610
R00617
R00621
R00650
R00654
R00658
R00660
R00662
R00669
R00670
R00671
R00674
R00678
R00679
R00691
R00694
R00704
R00705
R00706
R00707
R00708
R00709
R00710
R00711
R00713
R00714
R00717
R00720
R00722
R00731
R00734
R00742
R00747
R00748
R00749
R00750
R00751
R00754
R00761
R00762
R00768
R00774
R00776
R00782
R00783
R00785

R00787
R00789
R00791
R00798
R00801
R00816
R00817
R00818
R00823
R00825
R00829
R00832
R00835
R00837
R00841
R00842
R00847
R00848
R00851
R00858
R00868
R00875
R00878
R00880
R00885
R00888
R00891
R00894
R00896
R00897
R00899
R00904
R00907
R00908
R00921
R00924
R00926
R00927
R00930
R00931
R00935
R00936
R00937
R00939
R00940
R00942
R00944

R00945
R00946
R00959
R00963
R00965
R00966
R00977
R00985
R00986
R00987
R00988
R00994
R00996
R00997
R01001
R01011
R01015
R01025
R01030
R01036
R01041
R01049
R01051
R01054
R01056
R01057
R01058
R01061
R01064
R01067
R01068
R01070
R01071
R01072
R01073
R01074
R01078
R01082
R01083
R01085
R01086
R01088
R01090
R01106
R01117
R01122
R01126

R01127
R01130
R01132
R01135
R01137
R01138
R01150
R01152
R01154
R01155
R01158
R01163
R01168
R01171
R01172
R01174
R01175
R01177
R01209
R01213
R01214
R01215
R01220
R01221
R01224
R01226
R01227
R01229
R01230
R01231
R01245
R01248
R01251
R01253
R01257
R01262
R01267
R01273
R01279
R01280
R01286
R01287
R01288
R01290
R01293
R01298
R01301

R01302
R01324
R01325
R01333
R01334
R01342
R01347
R01348
R01351
R01353
R01354
R01357
R01360
R01361
R01364
R01372
R01373
R01374
R01384
R01388
R01392
R01394
R01395
R01397
R01398
R01404
R01406
R01416
R01419
R01431
R01432
R01434
R01446
R01466
R01470
R01492
R01512
R01513
R01514
R01518
R01519
R01520
R01521
R01528
R01529
R01530
R01541

R01542
R01557
R01560
R01569
R01579
R01600
R01602
R01621
R01623
R01626
R01631
R01632
R01639
R01641
R01648
R01655
R01658
R01664
R01665
R01676
R01677
R01687
R01699
R01708
R01714
R01715
R01716
R01717
R01718
R01724
R01731
R01736
R01737
R01739
R01741
R01745
R01747
R01752
R01764
R01768
R01770
R01771
R01773
R01775
R01776
R01779
R01786

R01787
R01795
R01799
R01800
R01801
R01804
R01818
R01819
R01825
R01826
R01827
R01829
R01830
R01845
R01855
R01856
R01857
R01858
R01859
R01868
R01870
R01873
R01874
R01887
R01896
R01899
R01900
R01901
R01904
R01909
R01931
R01933
R01934
R01936
R01939
R01940
R01954
R01959
R01968
R01975
R01976
R01977
R01986
R01990
R01993
R02000
R02003

R02014
R02016
R02017
R02018
R02019
R02020
R02021
R02022
R02023
R02024
R02025
R02029
R02030
R02032
R02034
R02035
R02036
R02055
R02059
R02060
R02061
R02085
R02090
R02093
R02100
R02101
R02102
R02103
R02110
R02111
R02142
R02143
R02164
R02166
R02173
R02194
R02196
R02199
R02235
R02236
R02237
R02241
R02243
R02269
R02272
R02274
R02279

R02282
R02283
R02286
R02288
R02291
R02300
R02301
R02320
R02322
R02323
R02325
R02326
R02328
R02331
R02340
R02352
R02353
R02363
R02377
R02382
R02383
R02404
R02407
R02408
R02412
R02413
R02415
R02422
R02423
R02425
R02433
R02472
R02473
R02487
R02488
R02491
R02519
R02521
R02527
R02529
R02531
R02532
R02536
R02537
R02540
R02549
R02558

R02565
R02566
R02568
R02569
R02570
R02571
R02577
R02601
R02602
R02603
R02604
R02613
R02619
R02649
R02658
R02661
R02662
R02668
R02670
R02672
R02678
R02685
R02695
R02697
R02718
R02719
R02720
R02722
R02735
R02736
R02739
R02740
R02747
R02750
R02752
R02756
R02762
R02777
R02780
R02783
R02788
R02797
R02804
R02864
R02908
R02914
R02918

R02919
R02925
R02940
R02957
R02964
R02971
R02985
R02991
R03004
R03005
R03008
R03012
R03018
R03026
R03027
R03033
R03035
R03038
R03045
R03050
R03051
R03066
R03067
R03083
R03084
R03093
R03096
R03098
R03102
R03103
R03105
R03106
R03119
R03132
R03145
R03154
R03158
R03165
R03172
R03174
R03177
R03178
R03180
R03181
R03182
R03191
R03192

R03193
R03194
R03197
R03210
R03220
R03223
R03231
R03232
R03243
R03254
R03269
R03270
R03276
R03291
R03293
R03296
R03300
R03302
R03307
R03313
R03316
R03321
R03346
R03348
R03350
R03351
R03383
R03387
R03417
R03425
R03443
R03457
R03458
R03459
R03460
R03470
R03471
R03472
R03493
R03494
R03508
R03509
R03527
R03534
R03543
R03549
R03550

R03559
R03560
R03595
R03596
R03599
R03601
R03608
R03646
R03650
R03651
R03652
R03654
R03655
R03656
R03657
R03658
R03659
R03660
R03661
R03662
R03663
R03664
R03665
R03777
R03778
R03789
R03809
R03813
R03815
R03816
R03857
R03858
R03862
R03868
R03869
R03877
R03889
R03896
R03898
R03903
R03905
R03916
R03925
R03936
R03940
R03947
R03948

R03968
R03970
R03971
R03974
R03975
R03977
R03980
R03990
R03991
R04000
R04001
R04014
R04025
R04030
R04035
R04037
R04089
R04095
R04097
R04109
R04112
R04125
R04137
R04138
R04144
R04152
R04160
R04170
R04173
R04187
R04188
R04189
R04198
R04199
R04203
R04204
R04208
R04210
R04212
R04215
R04217
R04224
R04230
R04231
R04258
R04277
R04280

R04292
R04300
R04323
R04325
R04326
R04355
R04365
R04376
R04378
R04385
R04386
R04390
R04391
R04405
R04424
R04425
R04426
R04428
R04429
R04430
R04432
R04435
R04439
R04440
R04441
R04444
R04445
R04457
R04463
R04475
R04482
R04486
R04487
R04509
R04535
R04537
R04544
R04547
R04549
R04550
R04558
R04559
R04560
R04567
R04568
R04573
R04587

R04591
R04592
R04606
R04617
R04639
R04640
R04657
R04658
R04672
R04673
R04674
R04693
R04710
R04724
R04725
R04726
R04734
R04737
R04738
R04739
R04740
R04741
R04742
R04744
R04745
R04746
R04747
R04748
R04749
R04751
R04754
R04770
R04771
R04773
R04780
R04781
R04809
R04810
R04812
R04813
R04856
R04859
R04862
R04863
R04880
R04882
R04883

R04888
R04889
R04890
R04891
R04892
R04893
R04894
R04903
R04907
R04911
R04930
R04935
R04936
R04941
R04942
R04949
R04951
R04952
R04954
R04955
R04956
R04957
R04958
R04959
R04960
R04961
R04962
R04963
R04965
R04966
R04967
R04968
R04969
R04970
R04983
R04984
R04986
R04987
R04988
R04989
R04990
R04993
R04996
R04998
R05032
R05046
R05048

R05049
R05050
R05051
R05052
R05062
R05064
R05066
R05068
R05069
R05070
R05071
R05074
R05085
R05086
R05146
R05149
R05150
R05177
R05180
R05181
R05198
R05199
R05217
R05219
R05220
R05221
R05222
R05224
R05225
R05227
R05233
R05234
R05237
R05238
R05243
R05265
R05284
R05285
R05286
R05287
R05289
R05290
R05291
R05295
R05298
R05299
R05300

R05305
R05320
R05332
R05353
R05362
R05366
R05367
R05368
R05369
R05370
R05374
R05390
R05404
R05406
R05509
R05510
R05551
R05553
R05576
R05577
R05578
R05582
R05586
R05590
R05591
R05595
R05605
R05607
R05608
R05614
R05616
R05620
R05621
R05622
R05627
R05629
R05630
R05633
R05634
R05636
R05637
R05644
R05645
R05646
R05647
R05662
R05681

R05688
R05692
R05693
R05704
R05706
R05712
R05717
R05772
R05773
R05794
R05808
R05809
R05810
R05814
R05815
R05835
R05837
R05838
R05864
R05865
R05884
R06113
R06171
R06337
R06338
R06404
R06447
R06513
R06514
R06529
R06558
R06590
R06601
R06602
R06604
R06620
R06784
R06785
R06786
R06787
R06788
R06789
R06836
R06859
R06867
R06895
R06915

R06939
R06941
R06942
R06966
R06977
R06983
R06989
R06990
R07034
R07035
R07157
R07168
R07210
R07219
R07222
R07262
R07268
R07273
R07281
R07294
R07296
R07302
R07363
R07364
R07390
R07394
R07396
R07404
R07405
R07406
R07409
R07411
R07412
R07414
R07415
R07417
R07418
R07419
R07459
R07460
R07461
R07463
R07599
R07600
R07601
R07602
R07603

R07604
R07605
R07613
R07618
R07639
R07658
R07659
R07660
R07661
R07662
R07664
R07669
R07670
R07687
R07706
R07709
R07710
R07762
R07766
R07767
R07768
R07769
R07772
R07795
R07809
R07810
R07812
R07821
R07839
R07855
R07888
R07891
R07892
R07895
R07896
R07934
R07935
R07950
R07951
R08056
R08058
R08088
R08089
R08090
R08091
R08092
R08093

R08094
R08095
R08157
R08158
R08209
R08210
R08218
R08236
R08237
R08238
R08239
R08240
R08244
R08245
R08246
R08346
R08347
R08348
R08360
R08362
R08363
R08364
R08549
R08639
R08648
R08689
R08714
R08836
R08856
R08944
R09079
R09080
R09081
R09082
R09097
R09099
R09107
R09151
R09152
R09229
R09248
R09289
R09365
R09366
R09372
R09380
R09381

R09382
R09383
R09384
R09386
R09401
R09473
R09492
R09499
R09543
R09565
R09597
R09641
R09675
R09697
R09698
R09725
R09736
R09763
R09768
R09769
R09773
R09774
R09781
R09796
R09805
R09819
R09834
R09838
R09839
R09840
R09841
R09843
R09936
R09978
R10002
R10035
R10039
R10040
R10042
R10043
R10052
R10074
R10086
R10092
R10115
R10117
R10118

R10119
R10121
R10122
R10123
R10124
R10147
R10149
R10151
R10170
R10178
R10202
R10206
R10209
R10221
R10247
R10343
R10460
R10564
R10640
R10641
R10645
R10646
R10647
R10652
R10697
R10703
R10704
R10706
R10707
R10712
R10718
R10747
R10806
R10831
R10845
R10851
R10852
R10859
R10880
R10904
R10906
R10907
R10948
R10949
R10991
R10992
R10993

R10994
R10996
R10997
R10998
Rnew1
R02094
R07280
R09419
R02027
R04150
R05617
R05615
R06146
R03504
R04620
R04031
R08165
R08166
R00616
R01350
R02250
R02054
R01309
R05592
R10601
R05600
R10699
R02135
R09977
R01244
R03013
R04743
R04753
R03856
R03989
R01278
R04543
R01706
R05138
R05288
R05282
R05292
R05389
R00813
R02990
R01906
R02665

R01938
R01066
R03030
R01047
R01366
R00699
R00830
R03222